

Transport properties of rippled graphene

Maciej Zwierzycki*

Institute of Molecular Physics, Polish Academy of Sciences, Smoluchowskiego 17, 60-179 Poznań, Poland

(Dated: ver. 3)

The exceptionally high mobility of carriers in graphene is one of its defining characteristics, especially in view of potential applications. Therefore it is of both practical and fundamental importance to understand the mechanisms responsible for limiting the values of mobility. The aim of the paper is to study theoretically one such mechanism, *i.e.* scattering on ripples. The transport properties of rippled graphene are studied using single-band tight-binding model. Both the bond-length variation, corresponding to the vector potential in the effective mass picture, and fluctuating scalar potential are included in the formalism. The samples are modeled as self-similar surfaces characterized by the roughness exponent with values ranging from typical for graphene on SiO₂ to seen in suspended samples. The range of calculated resistivities and mobilities overlaps with experiment. The results presented here support the notion of rippling as one of the factors limiting the mobility.

PACS numbers: 72.80.Vp, 61.48.Gh, 61.48.Gh

I. INTRODUCTION

The enormous interest in graphene, a two-dimensional (2D) honeycomb lattice of carbon atoms discovered in 2004¹, has both fundamental and practical reasons. The electronic properties of graphene are related to the peculiar nature of its band states in the vicinity of the Fermi level. These states possess a linear dispersion and are described by effective Hamiltonian formally identical to that of relativistic massless particles (Dirac fermions) albeit with velocity 300 times lower than the speed of light.² This leads to a range of interesting phenomena like finite minimal conductivity, Klein paradox (*i.e.* tunneling with no attenuation) or the anomalous Quantum Hall Effect which can be observed even at room temperatures (see *e.g.* Ref. [3] for a review). The practical interest stems mostly from the fact that carriers in graphene, whose number and character (electrons or holes) can be modified by field effect, possess exceptionally high mobility. The values range from order of 10.000 – 20.000 cm²/(V · s) for exfoliated graphene on SiO₂ substrate to over 100.000 cm²/(V · s) for suspended samples,^{4,5} making graphene a strong candidate for use in ultra-fast electronic devices.^{6–9}

The precise mechanism limiting the mobility of carriers in graphene is still a matter of debate. The values and temperature dependence of mobilities measured in suspended samples (in the doped regime) seem to support the phonon scattering model.⁴ The situation is less clear in samples on substrate where little temperature dependence is observed. An often suggested source of scattering in the latter case are charged impurities, possibly located in the substrate.¹⁰ However, an experiment designed specifically to test this scenario failed to produce supporting results.¹¹ Another possibility is scattering induced by ripples,¹² which has been observed in both suspended¹³ and exfoliated samples.^{14–17} Theoretical studies indicate that ripples can be caused by direct interaction with the substrate,¹⁷ thermodynamical instability inherent to 2D systems^{18,19}, functionalisation *e.g.*

by OH groups²⁰ or doping.²¹ The picture which emerges is that of graphene as self-similar rippled membrane.

One way to characterize such structure is via height-correlation function $\langle (h(\mathbf{r}) - h(\mathbf{0}))^2 \rangle$ which exhibits r^{2H} scaling for small values of r and eventually saturates at twice the standard deviation of height, $std(h) = \sqrt{\langle h^2 \rangle}$ (we assume $\bar{h} = 0$). The scaling exponent H is related to the fractal dimension of the rippled surface and assumes values ranging from 0.5 for exfoliated¹⁵ to 0.7 – 1.0 for suspended^{18,19,22} samples. The larger values of H in the latter case indicate locally smoother structures. The lateral size of surface features can be characterized by the correlation length ξ , defined as rollover point of height-correlation function²³, varying between several and few tens of nanometers.^{15,17,19} Finally, the size of out of plane fluctuations can be described by standard deviation of height, $std(h)$, usually equal to few Angstroms.

The most direct mechanism by which rippling modifies the electronic structure of graphene is the alteration of bond lengths (and consequently hopping integrals). Interestingly, in the effective mass approximation the resulting modifications to the Hamiltonian have a form of a random gauge field,^{24–26} whose presence may be responsible for suppression of weak localization observed in some graphene samples.²⁷ Furthermore the presence of ripples can lead to the fluctuations of charge density and in particular formation of electron and hole puddles in globally neutral samples. Gibertini *et al.*²⁸ calculated deformation potential for geometries obtained from Monte Carlo simulations^{18,22} and found it and the local charge density to vary on length scale of 1 – 2 nm with no apparent correlation to the height variation.²⁹ Similar length scales were also obtained in *ab initio* calculations of Ref. 30. Kim and Castro²⁰ and Gazit³¹ on the other hand obtained close correlation between the charge fluctuations and the local curvature of the graphene sheet. In this case the effective scalar potential varies on the length scales comparable to the coherence length. In all cases the amplitudes of the scalar potential variation were on the scale of tens of meV. On experi-

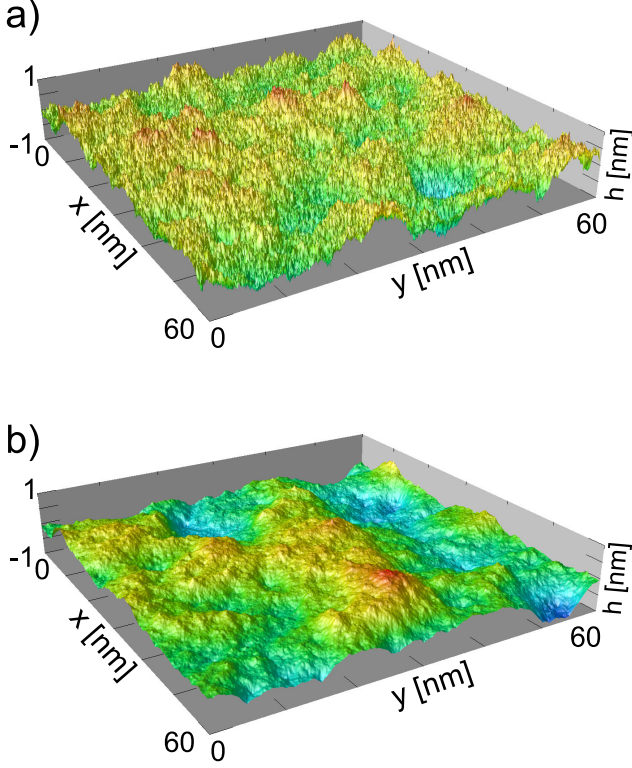


Figure 1. Two examples of surfaces generated using diamond-square algorithm. Scaling exponent H was set to 0.5 and 1.0 in a) and b) panels respectively. Standard deviation $std(h) = 3 \text{ \AA}$ was used in both cases.

mental side, electron and hole puddles were observed in scanning tunneling microscopy (STM) studies. However, the interpretation of their origin is a matter of ongoing discussion.^{32,33}

While the qualitative estimate of scattering rates associated with ripples were presented in Ref. 12, little in a way of explicit calculations of transport properties is present in the literature to date. Simple one-dimensional models were studied in Refs. 34 and 35. More sophisticated structural models were used in Refs. 36 and 37 but the effect of rippling was found to be modest compared to scattering on charged impurities. In both cases the modeling of the ripples was tailored to the specific case of relatively smooth structures of Ref. 18, characterized by $H = 1$. The aim of the present contribution is to study the transport properties for the structures in the whole range of H and $std(h)$ values. In the following paragraphs I will outline the details of the method of calculations and then present the results for both ballistic and diffusive regimes. Based on these I argue that the scattering on ripples has measurable impact on transport properties and leads in fact to resistance and mobility values compatible with experimental data.

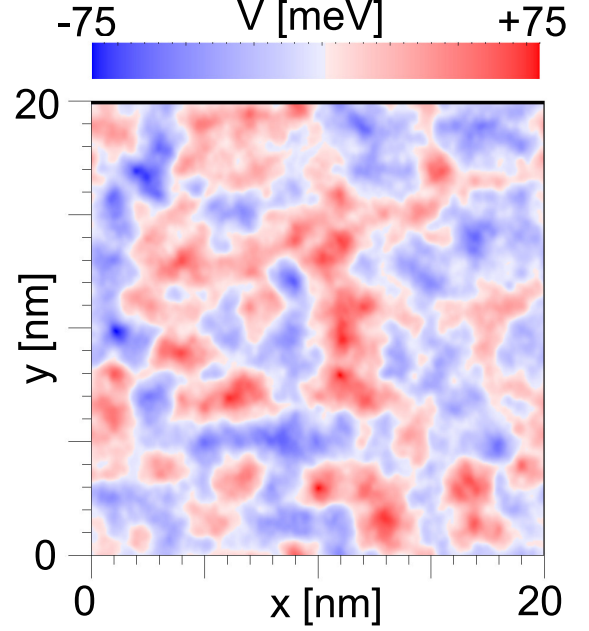


Figure 2. Scalar potential generated using diamond-square algorithm with $H = 1.0$ and $std(V_s) = 50 \text{ meV}$ using tiles of $2 \times 2 \text{ nm}$ (type A).

II. METHOD

The calculations were performed using a single-band tight-binding model with hopping restricted to nearest neighbors only. The effect of rippling was included in the Hamiltonian by modification of the hopping constants. A simple scaling formula was adopted to this end

$$t(r) = t_0 (r/a_0)^{-3} \quad (1)$$

where r is the interatomic distance, $a_0 = 1.42 \text{ \AA}$ is equilibrium lattice constant and $t_0 = t(a_0)$ equals -2.8 eV . The choice of scaling formula is further discussed in Appendix A. The scattering geometry was employed with system consisting of rippled region sandwiched between flat-graphene leads. The leads were assumed to be heavily doped with the Fermi energy located 1 eV over neutrality point. For such system transmission coefficients $t_{\mu\nu}$ between the incoming state ν in the left and outgoing state μ in the right electrode were calculated using wave function matching method.^{38,39} These were subsequently used in the Landauer-Büttiker formula for conductance

$$G_{LB} = \frac{e^2}{h} \sum_{\mu\nu} |t_{\mu\nu}|^2. \quad (2)$$

The self-similar landscape of the scattering region was generated using diamond-square algorithm,⁴⁰ described in the Appendix B, as multiples of $20 \times 20 \text{ nm}$ non-repeating tiles. This yields the correlation length of $\xi \approx 10 \text{ nm}$. The exponent H and $std(h)$ were adjustable parameters. Two examples of generated surfaces

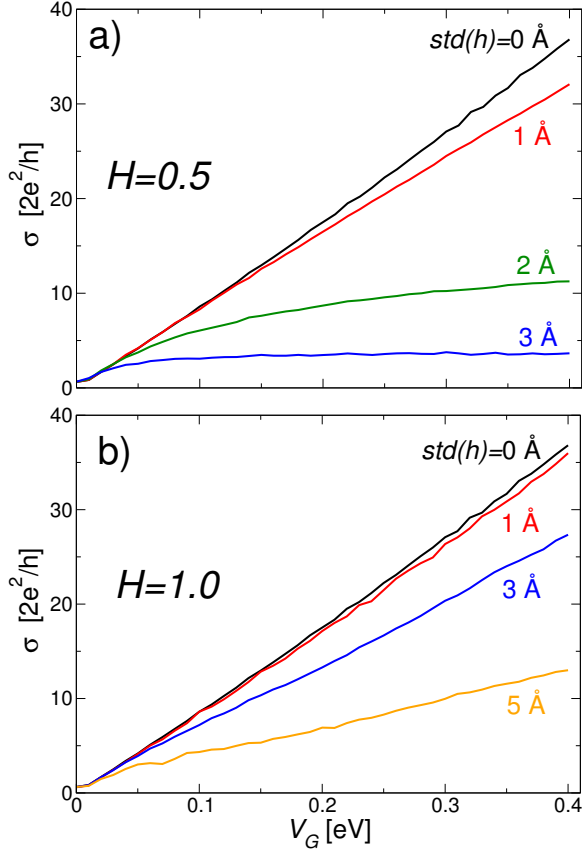


Figure 3. Conductivity $\sigma = G_{LB} \frac{L}{W}$ of the scattering region with $L = 100$ nm and $W = 20$ nm calculated as a function of V_G , the distance between the Fermi level and the neutrality point in the scattering region. Different curves correspond to the different values of $std(h)$.

are shown in Fig. 1. The honeycomb lattice of graphene was mapped onto the resulting surface with no adjustments to the in-plane positions of carbon atoms.

In some calculations a fluctuating scalar potential, included via the on-site elements of the tight-binding Hamiltonian, was taken into account. In contrast to Refs. 20, 28, 30, 31, and 41 where the calculated local potentials were explicitly dependent on the geometry, a simplified approach was adopted here. The potentials were generated independently, using the same algorithm as geometry, with height replaced by local potential. Two different tile sizes were employed, 2×2 and 20×20 nm, in order to create the potentials varying over shorter (*type A*) or longer (*type B*) length scales. The $H = 1$ exponent and additional averaging over neighbors was used so as to ensure the smoothness of resulting potentials. An example is shown in Fig. 2.

In all the calculations the transport was assumed to be along armchair direction and periodic boundary conditions with period W between 40 and 80 nm were used in the lateral (zigzag) direction. All the results presented in the following section were averaged over several tens realizations of the scattering region.

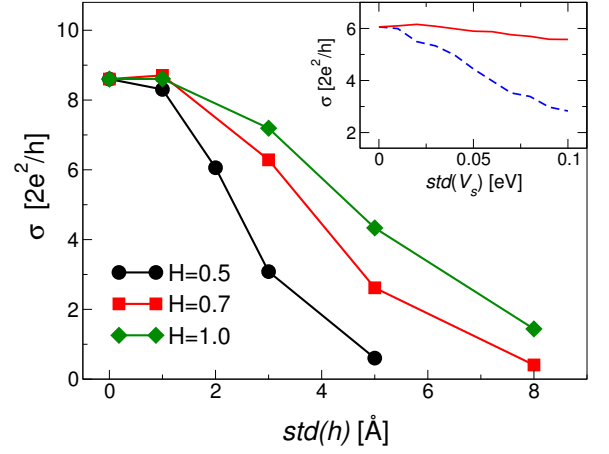


Figure 4. Conductivity as function of $std(h)$ for fixed $V_G = 0.1$ eV and different values of scaling exponent H . The inset: Conductivity as function of the standard deviation of scalar potential $std(V_s)$ for $H = 0.5$, $std(h) = 2$ Å and $V_G = 0.1$ eV. The results for *type A* (solid line) and *type B* (dashed line) potentials are presented.

III. RESULTS

In Fig. 3 the calculated conductivity $\sigma = G_{LB} \frac{L}{W}$ (for $L = 100$ nm and $W = 20$ nm) is shown as a function of a distance between the Fermi level and the neutrality point⁴² in the scattering region. This quantity, V_G , would be controlled by gate voltage in experiment. The convention used here is that positive values mean electron doping in the central part. It is immediately apparent that the conductance can be significantly lowered by the presence of the ripples. The effect increases for higher values of $std(h)$. Additionally the functional dependence of σ can also change and deviate from $\sigma \sim V_G$, typical for ballistic regime, as seen most clearly in Fig. 3a. Comparison of results obtained for $H = 0.5$ and 1.0 reveals that the back-scattering is greatly reduced in the latter case. This correlates with the structures characterized by higher H values being locally smoother (see Fig. 1). This point is further illustrated in Fig. 4 where the conductivities for three values of H are shown, for a fixed value of $V_G = 0.1$ eV (corresponding to $n = 10^{12} \text{ cm}^{-2}$ in flat graphene), as function of $std(h)$. The descent of the curves gets slower with increasing H , however even for $H = 1$, the effect is non-negligible. The dependence of conductivity on the standard deviation of the scalar potential, $std(V_s)$, is presented in the inset of Fig. 4 for $H = 0.5$ and $std(h) = 2$ Å. One sees that of the two model potentials, the “long-wavelength” type B has significantly stronger effect.

Interestingly, the region around neutrality point ($V_G \approx 0$) in Fig. 3 seems not to be affected by rippling. This is confirmed in Fig. 5 where the minimal conductance, $\sigma_{min} = \sigma(V_G = 0)$ is shown as a function of H and $std(h)$. The main surface plot corresponds to the case with no additional scalar potential. We observe that σ_{min} assumes

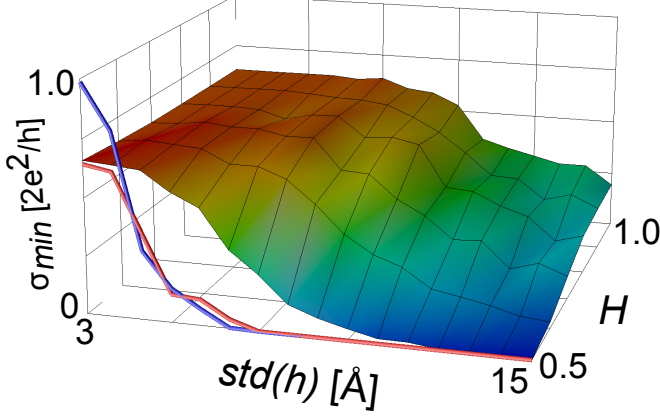


Figure 5. Minimal conductivity $\sigma_{min} = \sigma(V_G = 0)$ plotted as function of H and $std(h)$. The plateau values correspond to the universal value of $\sigma_{min} \approx \frac{4e^2}{h\pi}$. No scalar potential was present for the main surface plot. The results including fluctuating scalar potential were shown as red and blue lines for *type A* and *type B* potentials (with $std(V_s) = 0.05$ eV and $H = 0.5$) respectively.

the values close to the *universal* value of $\frac{4e^2}{h\pi}$, predicted for flat graphene,⁴³ over large plateau and decreases only for $std(h)$ exceeding H -dependent threshold value. Increasing the length of the scattering region (L) yields essentially same plateau region (results not shown) with a steeper descent outside. Adding the *type A* scalar potential does not, for $std(V_s) \lesssim 0.1$ eV, change the value of minimal conductance but reduces the size of the plateau. Exemplary results are shown in Fig. 5 using the red line for $H = 0.5$ and $std(V_s) = 0.05$ eV. The *type B* potential, which varies laterally on the same length scale as structural corrugations, is capable of changing not only stability but also the value of minimal conductance as demonstrated by the blue curve in Fig. 5 (same parameters apply). The observed increase of σ_{min} in the presence of the slow varying scalar potential can be qualitatively understood by noticing that in this case a carrier travels through a series of locally conductive regions (*i.e.* electron and holes puddles). For specific combinations of H , $std(h)$ and $std(V_s)$, σ_{min} can achieve a value of $\frac{4e^2}{h}$ often seen in exfoliated samples.² It should be noted however, that such values are no longer universal in my calculations, *i.e.* in addition to above mentioned variables they also depend on sample dimensions.

Following the usual convention the results of Figs. 3 and 5 were presented as *conductivities*, σ . It should be understood, however, that these results characterize a specific sample of given dimensions rather than bulk of a material. In fact, a naive attempt to extract conductivity or resistivity, as featured in Ohms law, from Eq. (2) is destined to fail as Landauer-Büttiker formula yields a finite resistance of a scattering region even in $L = 0$ limit.^{44,45} On the other hand one expects that if the scat-

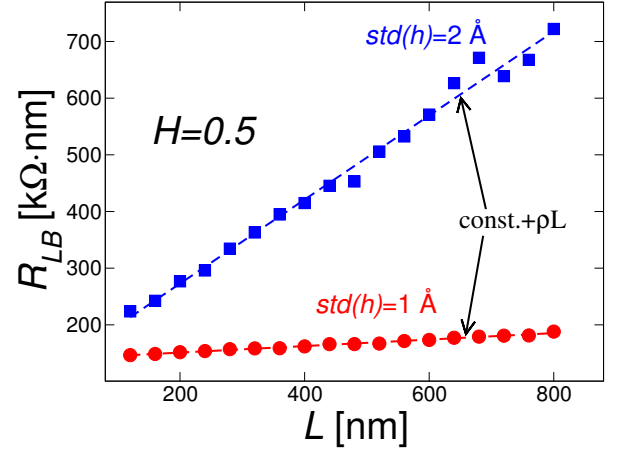


Figure 6. The illustration of the fitting procedure described in the text. The points on the plot are calculated values of $R_{LB} = G_{LB}^{-1}$ for $H = 0.5$ and $std(h)$ equal to either 1 Å (red circles) or 2 Å (blue squares) respectively. The dashed lines are the results of the least square fit, as described by Eq. (3).

tering region is sufficiently disordered, the overall resistance calculated as inverse of Eq. (2) should contain a contribution which scales linearly with L .⁴⁶ Therefore by calculating $G_{LB}^{-1}(L)$ and performing a least square fit to

$$R_{LB} = G_{LB}^{-1}(L) = const. + \rho \cdot L \quad (3)$$

it is possible to estimate resistance appropriate for ohmic regime. A constant term is, in present case, expected to be close to the inverse of Sharvin conductance,^{44,45} $G_{Sh} = \frac{e^2}{h}N$, proportional to the number of current carrying modes in the scattering region. The procedure is illustrated in Fig. 6 for $H = 0.5$ and $std(h) = 1$ and 2 Å. The resistivities obtained using Eq. (3) and $R_{LB}(L)$ calculated for lengths of up to $L = 800$ nm, are shown in Fig. 7. No calculations were performed for $H = 1.0$ and $std(h) < 3$ Å because the weak scattering in this case makes it difficult to reach the linear scaling regime. Once again the potential shift of the scattering region was set to $V_G = 0.1$ eV. As expected we observe that resistivity increases with $std(h)$ but decreases with growing H in qualitative agreement with Fig. 3. The inset of Fig. 7 shows the dependence of resistivity (for $std(h) = 1$ Å and $H = 0.5$) on the magnitude $[std(V_s)]$ of the scalar potential. We observe that additional scattering on fluctuating scalar potential can substantially increase resistivity, especially in the case of slow varying *type B* potential. Only very modest increase is seen for short-wavelength *type A* potential. This situation is analogous to the results for ballistic regime shown in the inset of Fig. 4. The range of calculated values overlaps with the experimentally observed range.^{1,4,5,11}

Having calculated resistivity we can now estimate the mobilities, μ , corresponding to Fig. 7. Using $\rho^{-1} = en\mu$ and assuming $n = 10^{12} \text{ cm}^{-2}$, appropriate for flat graphene with a chosen V_G , we obtain the values of μ

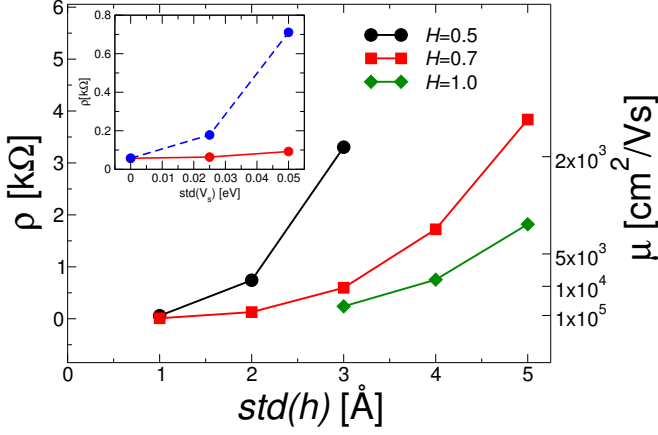


Figure 7. Resistivity calculated using Eq. (3) for different values of roughness exponent H , as function of $std(h)$. $V_G = 0.1 \text{ \AA}$ was used in all cases. The lines are guides to the eye only. The values of the corresponding mobilities can be read using the scale on the right vertical axis. *The inset:* Resistivity as function of $std(V_s)$ calculated with the inclusion of *type A* (solid line) and *type B* (dashed line) scalar potentials. $H = 0.5$ and $std(h) = 1 \text{ \AA}$ was used for both cases.

which can be read from the scale on the right vertical axis in Fig. 7. The STM studies reveal that exfoliated graphene on SiO_2 substrate is characterized by $H \approx 0.5$ and $std(h) \approx 2 - 3 \text{ \AA}$. This range of parameters corresponds in my calculations to the mobility in $\mu = 2.000 - 8.000 \frac{\text{cm}^2}{\text{V}\cdot\text{s}}$ range which is somewhat less than experimental values, typically equal to $10.000 - 20.000 \frac{\text{cm}^2}{\text{V}\cdot\text{s}}$.² The values of mobility are even more underestimated for the range of parameters corresponding to suspended graphene flakes, where simulations^{18,19,22} predict $H \approx 0.7 - 1.0$ and $std(h)$ of several Angstroms. This puts the calculated mobilities (see corresponding curves in Fig. 7) in the $10^3 \frac{\text{cm}^2}{\text{V}\cdot\text{s}}$ range, whereas much higher values of $100.000 \frac{\text{cm}^2}{\text{V}\cdot\text{s}}$ and more were reported experimentally.^{4,5} One possible reason for overestimation of scattering strength in my calculations may be the lack of structural relaxation in the model. It has been in fact demonstrated in the literature that relaxation of internal strain leads to the substantial reduction of the effect of rippling on electronic structure of the sample.⁴⁷

IV. CONCLUSIONS

In this paper I have studied the transport properties of rippled graphene using structural model parameterised by the scaling exponent H and the standard deviation $std(h)$ of the out-of plane positions of carbon atoms. Both in ballistic and ohmic regime a substantial reduction of conductivities was found already for relatively modest amplitudes of corrugation. The range of resistivities and mobilities calculated in ohmic regime over-

laps with experimental values. The mobility is however consistently underestimated when direct comparison is being made, possibly because of the limitations of the structural model. The value of minimal conductivity was found to be largely unchanged and equal to universal value $\sigma_{min} = \frac{4e^2}{h\pi}$ when only the effect of changing bond lengths was considered. The fluctuating scalar potential was found to decrease conductance for doped samples and increase the minimal conductance for globally neutral samples. In conclusion, the results presented in this paper support the notion that the rippled induced scattering is one of the important factors limiting the mobility of carriers in graphene.

ACKNOWLEDGMENTS

This work was supported by the Polish Ministry of Science and Higher Education as a research project No. N N202 199239.

Appendix A: The Scaling of The Hopping Constant

A simple formula for the scaling of the hopping constant used throughout the paper

$$t(r) = t_0 \left(\frac{r}{a_0} \right)^{-3} \quad (\text{A1})$$

is a special case of a general $t_{ll'} \sim r^{-l-l'-1}$ scaling (with $l = l' = 1$ for graphene π -band) motivated in turn by the scaling properties of the Hamiltonian of Linear Muffin Tin Orbital (LMTO)⁴⁸ method. Other choices, frequently utilized in the literature, include a quadratic scaling suggested by Harrison⁴⁹

$$t(r) = t_0 \left(\frac{r}{a_0} \right)^{-2} \quad (\text{A2})$$

or a more involved formula of Pereira *et al.*⁵⁰

$$t(r) = t_0 e^{-3.37 \left(\frac{r}{a_0} - 1 \right)} \quad (\text{A3})$$

The performance of all three scaling formulas is compared in Fig. 8 for both contracted (middle panel) and expanded (bottom panel) lattice constant. Additionally the results of tight-binding (TB) calculations were benchmarked against *ab-initio* Full Potential Linearized Augmented Plane Wave Method (FP LAPW).⁵¹ From the results shown in Fig. 8 it is clear that none of the formulas is consistently better than the other two. In the case of contracted lattice constant the best agreement between *ab initio* and TB results is given by Eq. (A2) with the other two being indistinguishable. However, the situation is reversed for expanded lattice constant when the *ab initio* bands are best reproduced by either Eq. (A3)

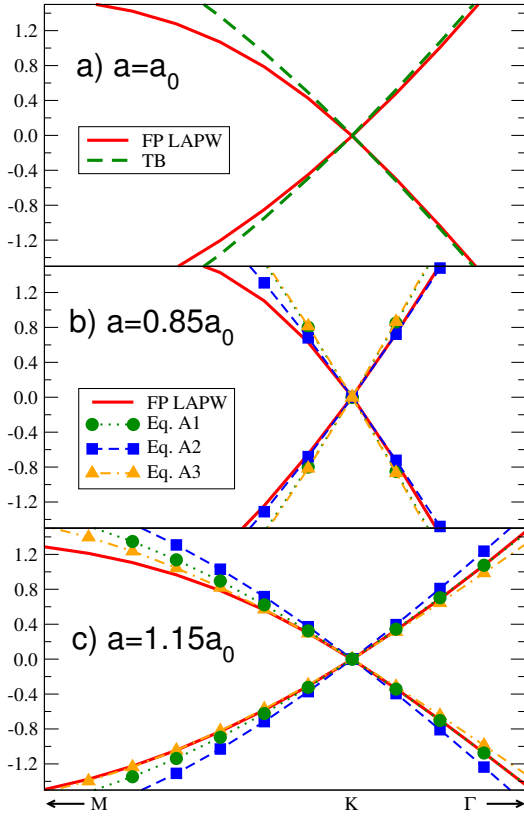


Figure 8. Graphene band structure around K-point calculated using tight-binding (TB) model and *ab initio* FLAPW method with lattice constant being a) at equilibrium value; b) contracted and c) expanded. The results of the three scaling formulas discussed in the Appendix A coincide in panel a) and are marked using circles (●), squares (■) and triangles (▲) for Eq. (A1), (A2) and (A3) respectively.

(along $M-K$ direction) or Eq. (A1) (along $K-\Gamma$) with Eq. (A2) clearly the worst of the three.

In the effective mass approximation, as used *e.g.* in Refs. 24–26, a linear scaling of the hopping constant is assumed and only the slope, usually parameterized as logarithmic derivative

$$\beta = - \left. \frac{d \ln t}{d \ln r} \right|_{r=a_0},$$

enters the theory. In this picture the Eqs. (A1), (A2), (A3) correspond to β equal to 3, 2 and 3.37 respectively. The theoretical and experimental estimates of β values found in the literature range between 1.1 and 3.6.⁵²

Appendix B: Diamond – Square Algorithm

The diamond-square algorithm, first proposed in Ref. 40, is an iterative procedure for generating fractal landscapes with chosen value of scaling exponent H . Consider a square with some predefined (possibly zero)

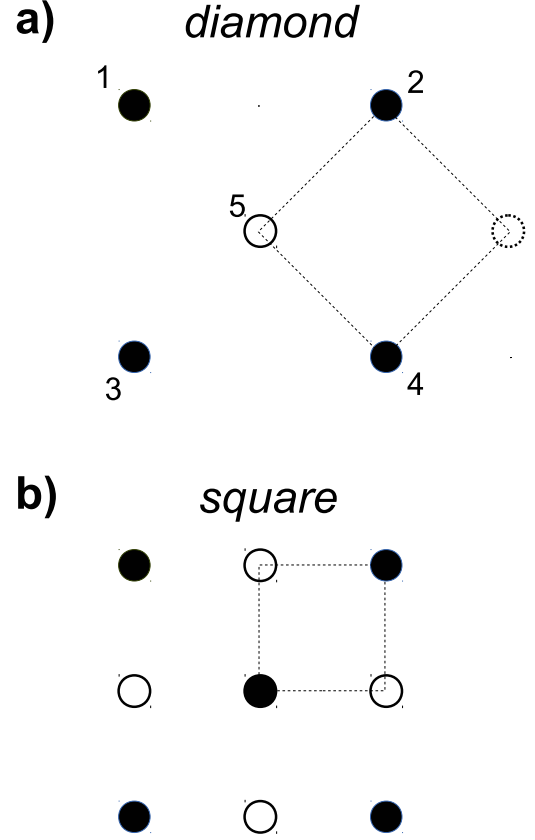


Figure 9. The two steps of diamond-square algorithm. The full circles (●) indicate points which values are known at the beginning of a step. The values of the points marked with empty circles (○) are calculated during the step. The dashed figures explain the name of each step.

corner values. The first iteration, shown in Fig. 9, consists of two steps:

- *diamond*: the central value of the square is calculated as

$$h_5 = \sum_{i=1 \dots 4} h_i + \text{rand}(d)$$

where $\text{rand}(d)$ is a random variable with normal distribution⁵³ centered at zero and standard deviation equal to d ,

- *square*: here one calculates the central values of the diamonds in analogous fashion.

Cyclic boundary conditions can be used in the first iteration or alternatively one can skip the points outside of the original rectangle. Both steps are repeated required number of times for squares and diamonds with dimensions halved in each iteration. Importantly, after each iteration the standard deviation of the random variable is reduced according to

$$d = \frac{d}{2^H}$$

thus enforcing required scaling properties. The scaling exponent H is related to the fractal dimension D of the structure via $D = 3 - H$.

It is easy to generalize the algorithm so that it works with rectangles consisting of multiple square tiles. This is the approach adopted in the paper, with the size of a basic tile equal to 20×20 nm. Thus obtained set of h was

renormalized so as to ensure $\bar{h} = 0$ and desired value of the standard deviation $std(h)$. The number of iterations were set to 8 resulting in a square grid with neighboring points being about 0.7 \AA apart, that is approximately half of interatomic distance in graphene. The hexagonal lattice of graphene was then overlaid on the square-grid surface by setting appropriate heights. The in-plane coordinates were not modified.

-
- * maciej.zwierzycki@ifmpan.poznan.pl
- ¹ K. S. Novoselov, A. K. Geim, S. V. Morozov, D. Jiang, Y. Zhang, S. V. Dubonos, I. V. Grigorieva, and A. A. Firsov, *Science* **306**, 666 (2004).
 - ² K. S. Novoselov, A. K. Geim, S. V. Morozov, D. Jiang, M. I. Katsnelson, I. V. Grigorieva, S. V. Dubonos, and A. A. Firsov, *Nature* **438**, 197 (2005).
 - ³ A. H. Castro Neto, F. Guinea, N. M. R. Peres, K. S. Novoselov, and A. K. Geim, *Rev. Mod. Phys.* **81**, 109 (2009).
 - ⁴ K. I. Bolotin, K. J. Sikes, J. Hone, H. L. Stormer, and P. Kim, *Phys. Rev. Lett.* **101**, 096802 (2008).
 - ⁵ X. Du, I. Skachko, A. Barker, and E. Y. Andrei, *Nature Nanotechnology* **3**, 491 (2008).
 - ⁶ Y.-M. Lin, K. A. Jenkins, A. Valdes-Garcia, J. P. Small, D. B. Farmer, and P. Avouris, *Nano Letters* **9**, 422 (2009).
 - ⁷ L. Liao, Y.-C. Lin, M. Bao, R. Cheng, J. Bai, Y. Liu, Y. Qu, K. L. Wang, Y. Huang, and X. Duan, *Nature* **467**, 305 (2010).
 - ⁸ Y.-M. Lin, A. Valdes-Garcia, S.-J. Han, D. B. Farmer, I. Meric, Y. Sun, Y. Wu, C. Dimitrakopoulos, A. Grill, P. Avouris, and K. A. Jenkins, *Science* **332**, 1294 (2011).
 - ⁹ F. Schwierz, *Nature Nanotechnology* **5**, 487 (2010).
 - ¹⁰ S. Adam, E. Hwang, E. Rossi, and S. D. Sarma, *Solid State Communications* **149**, 1072 (2009).
 - ¹¹ L. A. Ponomarenko, R. Yang, T. M. Mohiuddin, M. I. Katsnelson, K. S. Novoselov, S. V. Morozov, A. A. Zhukov, F. Schedin, E. W. Hill, and A. K. Geim, *Phys. Rev. Lett.* **102**, 206603 (2009).
 - ¹² M. Katsnelson and A. Geim, *Philos. Trans. R. Soc. A* **366**, 195 (2008).
 - ¹³ J. C. Meyer, A. K. Geim, M. I. Katsnelson, K. S. Novoselov, T. J. Booth, and S. Roth, *Nature* **446**, 60 (2007).
 - ¹⁴ E. Stolyarova, K. T. Rim, S. Ryu, J. Maultzsch, P. Kim, L. E. Brus, T. F. Heinz, M. S. Hybertsen, and G. W. Flynn, *Proc. Natl. Acad. Sci. U.S.A.* **104**, 9209 (2007).
 - ¹⁵ M. Ishigami, J. H. Chen, W. G. Cullen, M. S. Fuhrer, and E. D. Williams, *Nano Letters* **7**, 1643 (2007).
 - ¹⁶ V. Geringer, M. Liebmann, T. Echtermeyer, S. Runte, M. Schmidt, R. Rückamp, M. C. Lemme, and M. Morgenstern, *Phys. Rev. Lett.* **102**, 076102 (2009).
 - ¹⁷ W. G. Cullen, M. Yamamoto, K. M. Burson, J. H. Chen, C. Jang, L. Li, M. S. Fuhrer, and E. D. Williams, *Phys. Rev. Lett.* **105**, 215504 (2010).
 - ¹⁸ J. H. L. A. Fasolino and M. I. Katsnelson, *Nature Materials* **6**, 858 (2007).
 - ¹⁹ N. Abedpour, M. Neek-Amal, R. Asgari, F. Shahbazi, N. Nafari, and M. R. R. Tabar, *Phys. Rev. B* **76**, 195407 (2007).
 - ²⁰ E.-A. Kim and A. H. C. Neto, *Europhys. Lett.* **84**, 57007 (2008).
 - ²¹ D. Gazit, *Phys. Rev. B* **79**, 113411 (2009).
 - ²² J. H. Los, M. I. Katsnelson, O. V. Yazyev, K. V. Zakharchenko, and A. Fasolino, *Phys. Rev. B* **80**, 121405 (2009).
 - ²³ The height correlation function typically scales like $\langle (h(\mathbf{r}) - h(0))^2 \rangle \sim 2 \langle h^2 \rangle (1 - e^{-(r/\xi)^{2H}})$.
 - ²⁴ F. Guinea, B. Horovitz, and P. Le Doussal, *Phys. Rev. B* **77**, 205421 (2008).
 - ²⁵ F. Guinea, M. I. Katsnelson, and M. A. H. Vozmediano, *Phys. Rev. B* **77**, 075422 (2008).
 - ²⁶ M. Vozmediano, M. Katsnelson, and F. Guinea, *Physics Reports* **496**, 109 (2010).
 - ²⁷ S. V. Morozov, K. S. Novoselov, M. I. Katsnelson, F. Schedin, L. A. Ponomarenko, D. Jiang, and A. K. Geim, *Phys. Rev. Lett.* **97**, 016801 (2006).
 - ²⁸ M. Gibertini, A. Tomadin, M. Polini, A. Fasolino, and M. I. Katsnelson, *Phys. Rev. B* **81**, 125437 (2010).
 - ²⁹ Longer length scales were obtained by the same group⁴¹ when their formalism was applied to the experimental structure of Ref. 16.
 - ³⁰ P. Partovi-Azar, N. Nafari, and M. R. R. Tabar, *Phys. Rev. B* **83**, 165434 (2011).
 - ³¹ D. Gazit, *Phys. Rev. B* **80**, 161406 (2009).
 - ³² A. Deshpande, W. Bao, F. Miao, C. N. Lau, and B. J. LeRoy, *Phys. Rev. B* **79**, 205411 (2009).
 - ³³ Y. Zhang, V. W. Brar, C. Girit, A. Zettl, and M. F. Crommie, *Nature Physics* **5**, 722 (2009).
 - ³⁴ A. Isacsson, L. M. Jonsson, J. M. Kinaret, and M. Jonson, *Phys. Rev. B* **77**, 035423 (2008).
 - ³⁵ M. Zwierzycki, *Acta. Phys. Pol. A* **121**, 1246 (2012).
 - ³⁶ J. W. Klos, A. A. Shylau, I. V. Zozoulenko, H. Xu, and T. Heinzel, *Phys. Rev. B* **80**, 245432 (2009).
 - ³⁷ W. Zhu and B. Lv, *Physics Letters A* **377**, 1649 (2013).
 - ³⁸ K. Xia, M. Zwierzycki, M. Talanana, P. J. Kelly, and G. E. W. Bauer, *Phys. Rev. B* **73**, 064420 (2006).
 - ³⁹ M. Zwierzycki, P. A. Khomyakov, A. A. Starikov, K. Xia, M. Talanana, P. X. Xu, V. M. Karpan, I. Marushchenko, I. Turek, G. E. W. Bauer, G. Brocks, and P. J. Kelly, *Phys. Stat. Sol. B* **245**, 623 (2008).
 - ⁴⁰ A. Fournier, D. Fussell, and L. Carpenter, *Commun. ACM* **25**, 371 (1982).
 - ⁴¹ M. Gibertini, A. Tomadin, F. Guinea, M. I. Katsnelson, and M. Polini, *Phys. Rev. B* **85**, 201405 (2012).
 - ⁴² The value of V_G is calculated assuming that rippling does not change the position of neutrality point.
 - ⁴³ J. Tworzydło, B. Trauzettel, M. Titov, A. Rycerz, and C. W. J. Beenakker, *Phys. Rev. Lett.* **96**, 246802 (2006).

- ⁴⁴ Y. V. Sharvin, Zh. Eksp. Teor. Fiz. **48**, 984 (1965), [Sov. Phys. JETP **21**, 655 (1965)].
- ⁴⁵ S. Datta, *Electronic Transport in Mesoscopic Systems* (Cambridge University Press, Cambridge, 1995).
- ⁴⁶ P. X. Xu and K. Xia, [Phys. Rev. B **74**, 184206 \(2006\)](#).
- ⁴⁷ T. O. Wehling, A. V. Balatsky, A. M. Tsvelik, M. I. Katsnelson, and A. I. Lichtenstein, [Europhys. Lett. **84**, 17003 \(2008\)](#).
- ⁴⁸ O. K. Andersen, O. Jepsen, and D. Glötzl, in *Highlights of Condensed Matter Theory*, International School of Physics ‘Enrico Fermi’, Varenna, Italy, edited by F. Bassani, F. Fumi, and M. P. Tosi (North-Holland, Amsterdam, 1985) pp. 59–176.
- ⁴⁹ W. A. Harrison, *Elementary Electronic Structure* (World Scientific, Singapore, 2004); A generalized version of Harrison’s scaling suggested in C. H. Xu, C. Z. Wang, C. T. Chan, and K. M. Ho, [J. Phys.: Condens. Matter. **4**, 6047 \(1992\)](#) does not bring consistent improvement in the present case.
- ⁵⁰ V. M. Pereira, A. H. Castro Neto, and N. M. R. Peres, [Phys. Rev. B **80**, 045401 \(2009\)](#).
- ⁵¹ As implemented in WIEN2k program: K. Schwarz, P. Blaha, and G. Madsen, [Computer Physics Communications **147**, 71 \(2002\)](#).
- ⁵² H. Suzuura and T. Ando, [Phys. Rev. B **65**, 235412 \(2002\)](#); A. H. Castro Neto and F. Guinea, [Phys. Rev. B **75**, 045404 \(2007\)](#); E. Cappelluti and G. Profeta, [Phys. Rev. B **85**, 205436 \(2012\)](#) and references therein.
- ⁵³ Alternatively a uniform distribution over $[-d, d]$ can be used.